Phase diagram of the uniaxial and biaxial soft–core Gay–Berne model

Roberto Berardi,[1,a)] Juho S. Lintuvuori,[2,b)] Mark R. Wilson,[2] and Claudio Zannoni[1]
[1]*Dipartimento di Chimica Fisica e Inorganica, Università di Bologna, viale Risorgimento 4, 40136 Bologna, Italy*
[2]*Department of Chemistry, Durham University, South Road, Durham DH1 3LE, United Kingdom*

(Received 29 June 2011; accepted 15 September 2011; published online 7 October 2011)

Classical molecular dynamics simulations have been used to explore the phase diagrams for a family of attractive–repulsive soft–core Gay–Berne models [R. Berardi, C. Zannoni, J. S. Lintuvuori, and M. R. Wilson, J. Chem. Phys. **131**, 174107 (2009)] and determine the effect of particle softness, i.e., of a moderately repulsive short–range interaction, on the order parameters and phase behaviour of model systems of uniaxial and biaxial ellipsoidal particles. We have found that isotropic, uniaxial, and biaxial nematic and smectic phases are obtained for the model. Extensive calculations of the nematic region of the phase diagram show that endowing mesogenic particles with such soft repulsive interactions affect the stability range of the nematic phases, and in the case of phase biaxiality it also shifts it to lower temperatures. For colloidal particles, stabilised by surface functionalisation, (e.g., with polymer chains), we suggest that it should be possible to tune liquid crystal behaviour to increase the range of stability of uniaxial and biaxial phases (by varying solvent quality). We calculate second virial coefficients and show that they are a useful means of characterising the change in effective softness for such systems. For thermotropic liquid crystals, the introduction of softness in the interactions between mesogens with overall biaxial shape (e.g., through appropriate conformational flexibility) could provide a pathway for the actual chemical synthesis of stable room–temperature biaxial nematics. © *2011 American Institute of Physics*. [doi:10.1063/1.3646310]

I. INTRODUCTION

Several families of complex liquid crystal systems, formed by large biomolecules, polymers or colloidal nanoparticles, exhibit a high degree of conformational flexibility. This allows for a significant amount of interpenetration of the *molecular surfaces* of the mesogenic species on close approach. In such cases, particle interactions cannot be properly represented by the standard repulsive interactions commonly used for rigid bodies. A short (and incomplete) list of these systems includes a class of biaxial nematic mesogens,[1,2] ultrasoft anisotropic colloidal systems (such as star polymers[3]), hydrogel nanoparticles,[4] soft microgels,[5] deformable colloidal particles,[6] dendrimers,[7] self–assembling protein clusters,[8] anisotropic nanoparticles with shape–memory,[9] and semiflexible viruses.[10]

The complexity of these systems currently defies detailed atomistic study but, from the point of view of their pair interactions, particles can be modelled at the simplest level by replacing the complete impenetrability of hard interactions[11] by weak short–range ("*soft*") repulsions. Here, a "*soft*" interaction potential mimics a soft *molecular surface*, allowing partial overlap of individual mesogenic species when closely packed.

The possibility of partial particle interpenetration is also particularly interesting from the simulation point of view, since it can help proper equilibration and formation of complex structures, avoiding "*kinetic locking*" of partially organised molecular structures. With this in mind, soft spherocylinders have recently been exploited, with a combination of soft and harder building blocks, for the simulation of dendrimers and polyphilic systems.[12–15] Strings of soft repulsive ellipsoids have also been used for modelling liquid crystals and their rheological properties.[16,17] Quite independently Allen and collaborators[18] have used another soft repulsive ellipsoid variant to study colloidal particles in liquid crystals, and nematic–isotropic interfaces.[19] Soft Gaussian–core repulsive ellipsoids potentials, forming various crystal structures as well as smectics and nematics, have also been proposed by Prestipino and Saija,[20,21] and Nikoubashman and Likos.[22]

For a variety of systems, attractive interactions cannot be neglected and the Gay–Berne (GB) potential in its uniaxial[23] or biaxial form[24,25] currently represents the *de–facto* standard attractive–repulsive molecular resolution model for the computer simulation of liquid crystals and self–assembling anisotropic materials[11,26,27] (see Ref. 28 for a review of the current Gaussian overlap and generalised GB potentials). We have recently proposed a soft–core (SC) version[29] of the general biaxial GB potential, where both the attractive and repulsive parts are maintained, while the steepness of the repulsive part of the potential can be varied. A preliminary investigation has shown that the potential can still form nematics and smectics, and when coupled with Hamiltonian replica exchange, can provide a considerable speed up in computer simulations. This soft–core GB potential has recently proved to be invaluable in the simulation of main

[a)]Author to whom correspondence should be addressed. Electronic mail: roberto.berardi@unibo.it.
[b)]Present address: School of Physics and Astronomy, The University of Edinburgh, James Clerk Maxwell Building, Mayfield Road, Edinburgh EH9 3JZ, United Kingdom.

chain liquid crystal swollen elastomers,[30] where equilibration of conventional models is very difficult.

When introducing a new feature (such as softness) in a known potential, a key problem is understanding how the changes to the potential affect the phases that can be obtained. In the current paper we present a molecular dynamics computer simulation study, which explores the isotropic, nematic, and marginally the smectic regions of the phase diagrams for uniaxial and biaxial ellipsoids with various degrees of softness, and also examines the effect of SC repulsions on mesogenic properties. In particular, since off–lattice hard–core models provide a good description of the entropic contribution to liquid crystalline behaviour, we have studied how the weakening of this repulsive contribution combines with anisotropic attractions towards the stabilisation of thermotropic mesogenic fluid phases, especially the uniaxial and the biaxial nematics.

A key quantity in estimating the relative importance of the attractive and repulsive contributions to the pair potential is the second virial coefficient B_2.[31,32] For protein and colloidal suspensions, this is particularly valuable because B_2 has been used to identify the range of conditions (leading to the right balance of attractions and repulsions) favourable for protein crystallisation as discussed by George and Wilson.[31] As B_2 is experimentally measurable,[33] and since the softness can in principle be tuned by appropriate coating of a colloidal nanoparticle with polymer chains (or other surface treatments), it is important to relate phase behaviour to B_2. This was achieved by Vliegenthart and Lekkerkerker[32] for simple spherical Lennard–Jones particles either of the standard 6–12 type or with the modified shorter range 18–36 form, with the results related to the earlier George and Wilson suggestions for proteins. Here we calculated numerically B_2 for the various potentials considered.

The plan of this paper is as follows: in Sec. II we provide the technical details of the computer simulations; in Secs. III A and III B we discuss the molecular dynamics and second virial results for uniaxial and biaxial SC ellipsoidal models, respectively, and compare them with those from the standard GB potential.[34,35] Conclusions are presented in Sec. IV.

II. SOFT–CORE MODEL AND COMPUTER SIMULATIONS

The potential used in this work is a soft–core (GBSC) version[29] of the standard GB model,[23–25] which describes the anisotropic and heterogeneous interaction between uniaxial and biaxial ellipsoidal particles. The SC variant of this potential has been obtained by replacing the steep repulsive branch of the U^{GB} energy with a constant–slope U^{SC} surface (see Figure 1), and smoothly seaming the two functional forms with a sigmoidal switching function

$$U^{\mathrm{GBSC}} = [1 - f(r, \boldsymbol{\omega})]\, U^{\mathrm{GB}}(r, \boldsymbol{\omega}) + f(r, \boldsymbol{\omega})\, U^{\mathrm{SC}}(r, \boldsymbol{\omega}), \tag{1}$$

where r is the centre–centre distance, and $\boldsymbol{\omega} \equiv (\boldsymbol{\omega}_1, \boldsymbol{\omega}_2, \boldsymbol{\omega}_{\mathbf{r}})$ stands, respectively, for the set of orientations (e.g., Euler angles, quaternions, cartesian matrices, . . .) of particles 1 and 2, and of the intermolecular vector $\mathbf{r}$. Particle–particle separations and energies are measured in σ_0 and ϵ_0 units. The GB interaction between two ellipsoidal particles is written as[23–25]

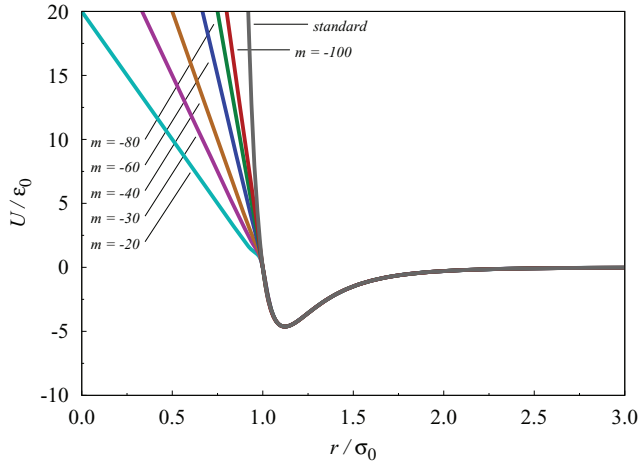

FIG. 1. Representative profiles for the uniaxial GBSC potential with $\sigma_x = \sigma_y = \sigma_c = 1\,\sigma_0$, $\sigma_z = 3\,\sigma_0$, and $\epsilon_x = \epsilon_y = 1\,\epsilon_0$, $\epsilon_z = 0.2\,\epsilon_0$, $\mu = 1$, $\nu = 3$, and slopes $m/(\epsilon_0\,\sigma_0^{-1}) = -100$, -80, -60, -40, -30, and -20. (See text for additional details.) The steepness for the logistic seaming function was $k = -70\,\sigma_0^{-1}$, and a threshold cut–off value $\|1 - f\| = 10^{-6}$ was used (see Ref. 29). The energy curves are relative to the *side–by–side* interaction of two parallel ellipsoids. A plot for the standard GB *side–by–side* interaction energy is also provided for comparison.

$$U^{\mathrm{GB}}(r, \boldsymbol{\omega}) = 4\epsilon_0\, \epsilon(\boldsymbol{\omega})[u^{12}(r, \boldsymbol{\omega}) - u^{6}(r, \boldsymbol{\omega})], \tag{2}$$

with $u(r, \boldsymbol{\omega}) = \sigma_c/(r - \sigma(\boldsymbol{\omega}) + \sigma_c)$. The shape $\sigma(\boldsymbol{\omega})$ and the interaction $\epsilon(\boldsymbol{\omega})$ terms control the anisotropic contact distance and potential wells. The SC repulsive energy has a linear dependence on the particle–particle separation[29]

$$U^{\mathrm{SC}}(r, \boldsymbol{\omega}) = m\,[r - \sigma(\boldsymbol{\omega})], \tag{3}$$

where $\sigma(\boldsymbol{\omega})$ is the anisotropic contact term of the GB potential. The sigmoidal seaming function is

$$f(r, \boldsymbol{\omega}) = \exp[k\,(r - \sigma(\boldsymbol{\omega}))]/(1 + \exp[k\,(r - \sigma(\boldsymbol{\omega}))]), \tag{4}$$

where the parameter k defines the steepness of the logistic function at its inflection point. The GB and SC surfaces are smoothly seamed along the locus $r = \sigma(\boldsymbol{\omega})$, $U^{\mathrm{GB}}(r, \boldsymbol{\omega}) = 0$ where the GB energy changes sign. This choice has two advantages: one physical, the other computational. The first one is that mesogenic properties (arising from the specific attractive–repulsive GB energy surface) are not greatly impaired if the softness is not very large compared to the original r^{-12} repulsive branch of the standard GB potential. The second one is that the SC energy term can be efficiently determined using quantities already computed for the evaluation of $U^{\mathrm{GB}}(r, \boldsymbol{\omega})$. Using this approach the GBSC potential can model either relatively soft particles that still do not interpenetrate (i.e., for temperatures giving liquid phases, this is effectively equivalent to having a vertical asymptote for $r - \sigma(\boldsymbol{\omega}) + \sigma_c = 0$), or very soft particles that

can strongly overlap. Further details on the computation of energies, forces, and torques for the GBSC potential can be found elsewhere.[29,36,37] Here, we concentrate on the physical properties of this coarse–grained model and deploy classical molecular dynamics (MD) simulations to assess the general effects of softness on the mesogenic properties of uniaxial and biaxial GBSC ellipsoids. The emphasis of this computer simulation work is on trends, so we study a large number of state points using relatively small samples and aim to locate phase transitions from changes of order parameters, radial correlation function, and visual inspection of the samples rather than from explicit free energy calculations. The latter one is indeed still quite demanding, even if we note some recent progress in this area.[38–40]

Classical MD simulations of $N = 1024$ particles have been performed with constant number of particles N, volume V, and temperature T, using a cubic box with periodic boundaries at dimensionless number density $\rho^* \equiv (N/V)\,\sigma_0^3 = 0.3$.[34] The velocity Verlet[41] and the quaternion–based[29,42,43] integrators for the classical translational and rotational equations of motion have been used with a dimensionless time step $\Delta t^* = (\epsilon_0 \sigma_0^{-2} m_0^{-1})^{1/2} \Delta t = 0.001$. Temperature has been controlled using a weak–coupling Berendsen thermostat,[44,45] with time constant $\tau_T^* = 10$. State points have been equilibrated for at least 200 k time steps and mean properties have been computed as block averages (with the corresponding rms errors) performed over 200 k time step runs with an initial sampling stride of 20 time steps (see the tables in the supplementary material[46] for a complete listing of these values). The MD simulations have been run on 3 GHz Intel Xeon 5160 cores, with a one 200 k time step run requiring ≈21 h, for a total of approximately 19 000 h for the 454 state points studied.

We have considered elongated Gay–Berne ellipsoids with two parametrisations (but same volume), which have been studied in the past in standard GB form: namely, uniaxial[34] (with $\sigma_x = \sigma_y = 1\,\sigma_0$, $\sigma_z = 3\,\sigma_0$, and $\epsilon_x = \epsilon_y = 1\,\epsilon_0$, $\epsilon_z = 0.2\,\epsilon_0$) and biaxial[35] (with $\sigma_x = 1.4\,\sigma_0$, $\sigma_y = 0.714\,\sigma_0$, $\sigma_z = 3\,\sigma_0$, and $\epsilon_x = 1.7\,\epsilon_0$, $\epsilon_y = 1\,\epsilon_0$, $\epsilon_z = 0.2\,\epsilon_0$). For both parametrisations the GB empirical tuning exponents μ, ν were $\mu = 1$ and $\nu = 3$. These models of thermotropic calamitic mesogens give isotropic, nematic, and smectic phases. The repulsive SC surfaces considered in this work are shown in Figure 1 for the *side–by–side* configuration, and have slopes m ranging from $m = -20\,\epsilon_0\,\sigma_0^{-1}$ (fairly soft) to $m = -100\,\epsilon_0\,\sigma_0^{-1}$ (scantly soft). The switching function was characterised by an inflection point of steepness $k = -70\sigma_0^{-1}$, and a threshold value $\|1 - f\| = 10^{-6}$ for its cut-off.

III. SIMULATION RESULTS

Before going into the details of our results for uniaxial and biaxial particles, we note that we have identified the isotropic–nematic (I–N) transition temperature as that of the state point with mean order parameter $\langle R_{0,0}^2 \rangle \geq 0.3$, while a transition to a biaxial (nematic) phase was assigned whenever $\langle R_{2,2}^2 \rangle \geq 0.1$. The spontaneous formation of layered structures, as characterised by peaks in the radial distribution function parallel to the director, $g(r_\parallel)$, and also visible in the snapshots of MD samples identifies the transition to smectic phases. All thermodynamical quantities have been expressed in their dimensionless form, e.g., mass m/m_0, energy U/ϵ_0, temperature $T/(k_B^{-1}\epsilon_0)$, pressure $P/(\sigma_0^{-3}\epsilon_0)$. Moreover, to verify if the various SC parametrisations provide similar liquid crystal stability ranges, we have plotted most observables against reduced temperature T/T_{IN}, where T_{IN} identifies the spontaneous I–N ordering transition (if any) for each parametrisation.

A. Uniaxial particles

The first family of SC systems considered are those based on a standard uniaxial GB model showing isotropic, nematic, and smectic phases.[34] These simulations allow us to study the effect of softness in an ellipsoidal GBSC model, as tuned by changing the slope m of the repulsive part of the potential (see Figure 1), on the capability of forming anisotropic ordered fluid phases by spontaneously aligning the principal molecular axis. Surprisingly, a small degree of softness ($m = -100\,\epsilon_0\,\sigma_0^{-1}$, and $m = -80\,\epsilon_0\,\sigma_0^{-1}$) stabilises the ordered phases, and the I–N transition is shifted to higher temperatures (T_{IN} increases by ≈52% for $m = -100\,\epsilon_0\,\sigma_0^{-1}$ and ≈38% for $m = -80\,\epsilon_0\,\sigma_0^{-1}$) compared to the standard GB model. For intermediate softnesses ($m = -60\,\epsilon_0\,\sigma_0^{-1}$ and $m = -40\,\epsilon_0\,\sigma_0^{-1}$) the I–N transition is still higher but now closer to the standard GB transition (respectively, ≈25% and ≈5%). In particular, the latter parametrisation closely follows the phase diagram of the standard GB in the smectic and nematic regions, and deviates only in giving a slightly higher I–N transition temperature. Increasing softness even more ($m = -30\,\epsilon_0\,\sigma_0^{-1}$ and $m = -20\,\epsilon_0\,\sigma_0^{-1}$) reduces the anisotropy of the GBSC model, destabilises the ordered phases with the effect that the I–N transition is now shifted to low temperatures (respectively, by ≈ −5% and ≈ −16%).

Comparing these MD simulation results with those for the standard core GB potential we see that, as the potential softness increases, the number of thermally accessible states with positive energies grows also, especially for $T/T_{IN} \geq 1$; leading to the mean potential energies becoming positive at high temperatures. As a consequence of this, all SC models have energies higher than the corresponding one for the standard GB model. The average dimensionless energy per particle $\langle U \rangle/\epsilon_0$ plotted for the various parametrisation against the reduced temperature (see Figure 2(a)) does not exhibit significant discontinuities across the temperature range, and the spontaneous ordering transitions appear to be either very weakly first order (or even of second order character).

The corresponding plot for the dimensionless pressure (Figure 2(b)) shows that the moderately SC models systematically exhibit a higher $\langle P \rangle\,(\sigma_0^{-3}\epsilon_0)$ than the standard GB parametrisation, while the even softer ones ($m/(\epsilon_0\,\sigma_0^{-1}) = -40$, -30, and -20) have in contrast a smaller average pressure. So, in SC systems the repulsive contribution arising from the virial can be either larger or smaller than that in the standard model. The unusual

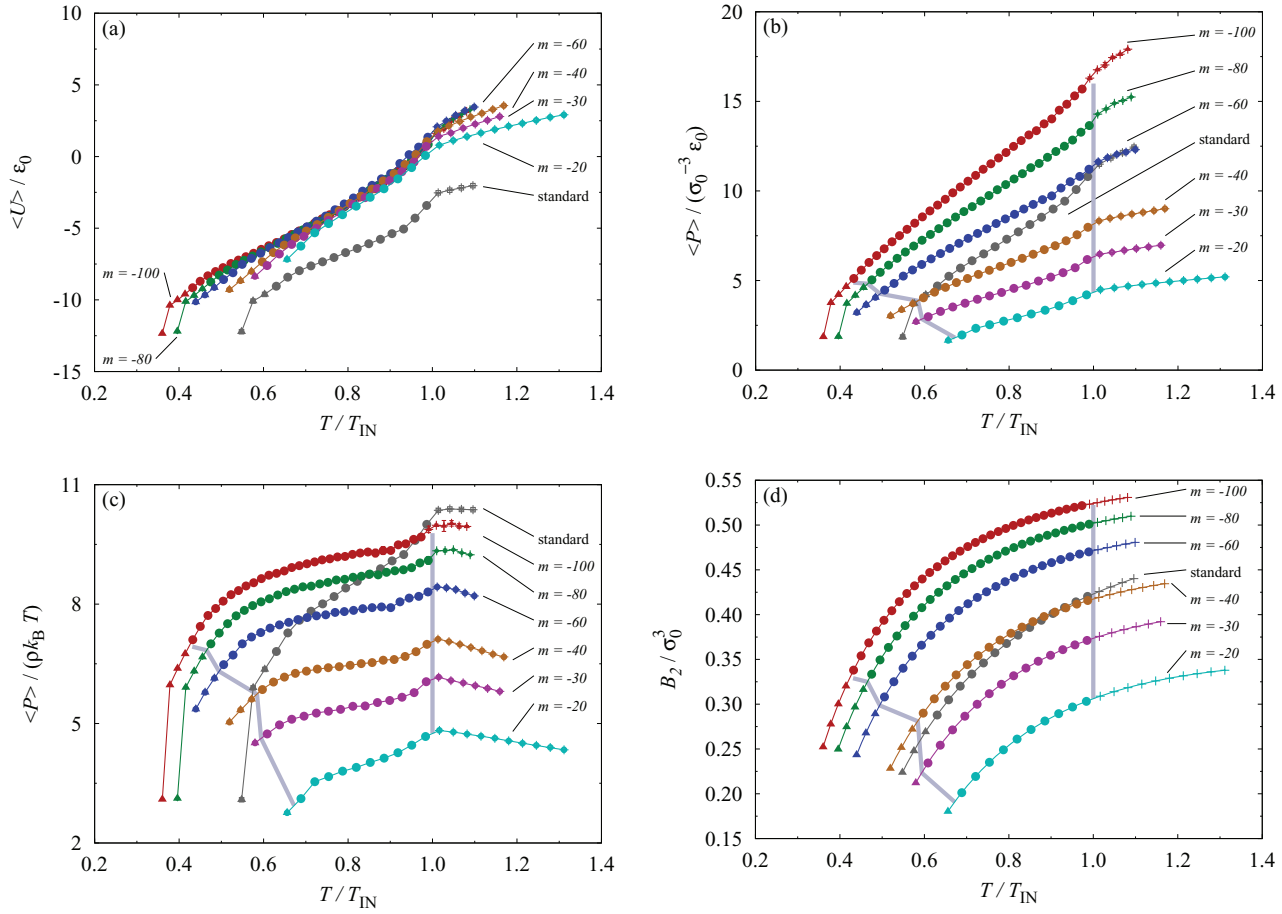

FIG. 2. The average dimensionless potential energy $\langle U\rangle/\epsilon_0$ (plate A), pressure $\langle P\rangle\,(\sigma_0^{-3}\epsilon_0)$ (plate B), compressibility factor $\langle P\rangle/(\rho k_B T)$ (plate C), and the second virial coefficient B_2 (plate D) plotted against the reduced temperature T/T_{IN} for uniaxial ellipsoids modelled either with the standard GB potential (see Ref. 34) or the GBSC parametrisation described in the text. The soft–core energy slopes were $m/(\epsilon_0\,\sigma_0^{-1}) = -100$, -80, -60, -40, and -30, while the logistic function steepness was $k = -70\,\sigma_0^{-1}$. The results from the NVT MD simulation of the standard uniaxial GB model (see Ref. 34) are also plotted. The rms errors computed, as described in the text, from a block average analysis of the simulation results (see supplementary material of Ref. 46) are also plotted as error bars, however, their size smaller than that of the symbols makes them hardly visible. For every SC parametrisation studied T_{IN} is the specific nematic–isotropic transition temperature, respectively, $T_{IN}/(k_B^{-1}\epsilon_0) = 5.55$, 5.05, 4.55, 3.85, and 3.45. The thick grey lines join the I–N and N–S_m transition temperatures for the GBSC models. The standard GB model has instead $T_{IN}/(k_B^{-1}\epsilon_0) = 3.65$. The state points have been computed from MD simulations in the NVT ensemble for $N = 1024$ particles samples at dimensionless density $(N/V)\,\sigma_0^3 = 0.3$.

behaviour in the pressure with respect to the standard case can be interpreted by considering the net balance in the virial between two competing effects: the profile of the GBSC potential for distances smaller than the seaming point, and the increasing number of thermally accessible low repulsive energy states in the liquid region of the phase diagram. A feature common to all parameterisations studied is that in the seaming region the GBSC potential energy is slightly steeper than the standard GB model, and this accounts for slightly (approximately 5% – 10%) stronger repulsions before the force drops to the constant SC value. In addition to that, for the uniaxial models with $m = -100\,\epsilon_0\,\sigma_0^{-1}$ and $m = -80\,\epsilon_0\,\sigma_0^{-1}$ the SC surface is still relatively steep and even though the population in the $r < \sigma(\boldsymbol{\omega})$ region is small, this also contributes towards raising the virial term in the pressure. As softness increases to $m = -40\,\epsilon_0\,\sigma_0^{-1}$ and larger values, the $r < \sigma(\boldsymbol{\omega})$ region becomes progressively more populated, but since this is accompanied at the same time by a large increase in the number of thermally accessible low repulsive energy states the combined effect is that of lowering the virial contribution to the pressure with respect to the standard GB model.

The compressibility factor $Z = \langle P\rangle/(\rho k_B T)$ (Figure 2(c)) allows an easier comparison of these properties for the various parametrisations: while the softer systems with $m/(\epsilon_0\,\sigma_0^{-1}) = -40$, -30, and -20 have a $\langle P\rangle/(\rho k_B T)$ ratio smaller than the one for the standard model over the entire temperature range (with the exception of a few low–temperature smectic points for $m = -40\,\epsilon_0\,\sigma_0^{-1}$), the moderately soft parametrisations with $m/(\epsilon_0\,\sigma_0^{-1}) = -100$, -80, and -60 show two different regions across the temperature range and give a smaller compressibility factor in the isotropic and low–ordered nematic range, while in the highly ordered nematic and smectic phases $\langle P\rangle/(\rho k_B T)$ become larger than the standard model. We also notice that for the SC systems the compressibility factor profiles have both a weaker temperature dependence and a similar shape, while being approximately parallel to each other.

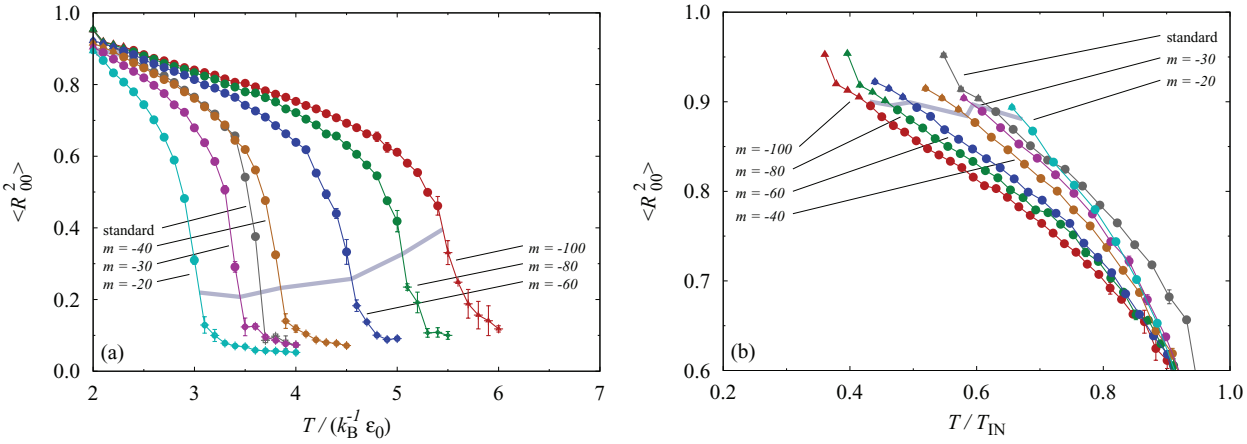

FIG. 3. The orientational order parameter $\langle R_{00}^2 \rangle$ plotted against dimensionless temperature $T/(k_B^{-1}\epsilon_0)$ (plate A), and reduced temperature T/T_{IN} (plate B), for the GBSC uniaxial ellipsoids of various softness $m/(\epsilon_0\,\sigma_0^{-1}) = -100, -80, -60, -40, -30$, and -20 as described in the text. (See the legend of Figure 2 for additional details.)

The change in balance between attractive and repulsive interactions, is in turn manifested by a change in the second virial coefficient B_2 as a function of temperature

$$B_2(T) = \frac{1}{2V_\omega}\int d\boldsymbol{\omega}_2 d\boldsymbol{\omega}_\mathbf{r} \times \int_0^\infty (1 - \exp[-U^{\mathrm{GBSC}}(r, \boldsymbol{\omega}_2, \boldsymbol{\omega}_\mathbf{r})/(k_B T)])\, r^2 dr, \tag{5}$$

where the first particle is kept fixed in the origin, and $V_\omega = 16\pi^2$ for uniaxial particles and $V_\omega = 32\pi^3$ for biaxial ones. A positive (or negative) B_2 indicates a dominance of repulsive (or attractive) interactions. We recall that in thermodynamic terms B_2 represents deviations from ideality in a gas resulting from pair interactions: $PV/(RT) = 1 + B_2(T)/V$. However, B_2 also plays a key role in colloidal suspensions[47] and polymer solutions. Here,[48] the osmotic pressure can be expanded in terms of concentration with B_2 identified as the second osmotic virial coefficient. In this work, we have evaluated B_2 via integration using Eq. (5) for our soft Gay–Berne potential (Figure 2(d)). Integrals over the orientations have been computed using 32 Gauss–Legendre points for each angular dimension. The introduction of a small degree of softness ($m/(\epsilon_0\,\sigma_0^{-1}) = -100, -80$, and -60) is clearly reflected in an increase in B_2, corresponding to a net repulsion integrated over angles, which in our case provides a rationale for the increase in stability of nematic phases for these potentials in comparison to the standard GB potential. Conversely, the softer variants of the GBSC potential have consistently smaller values of B_2 than seen for the standard Gay–Berne.

A more pronounced effect of softness was found for the average uniaxial orientational order parameter $\langle R_{0,0}^2 \rangle \equiv S = \langle [3(\mathbf{z}_i \cdot \mathbf{n})^2 - 1]/2 \rangle$, where $\mathbf{n}$ is the principal director, and $\mathbf{z}_i$ are the long molecular axes (all as unit vectors), and S is the standard symbol used in the Maier–Saupe model of nematics. The plot of $\langle R_{00}^2 \rangle$ against temperature (Figure 3(a)) shows the effect of softness on the spontaneous I–N transition temperatures. These curves are similar but not completely superimposable when plotted with respect to T/T_{IN}, as we can see from Figure 3(b). This plot shows that the SC systems consistently have smaller $\langle R_{00}^2 \rangle$ order parameters than the standard model at the same T/T_{IN}. This can be interpreted in terms of a decreased tendency to align arising from the weaker hard core repulsions and a reduced effective volume.

The position of the first maximum of the radial correlation function, $g(r)$ for nematic phases of standard and GBSC ellipsoids with similar orientational order parameter $\langle R_{00}^2 \rangle \approx 0.8$ (see Figure 4) is practically unaffected by the particle softness, while the second maximum shows a small shift towards larger separations. Correspondingly, the height of the maxima is lowered as m increases and the longer range structure in the fluid is smoothed out. The principal effect of softness on the radial correlation function appears to be the progressive population of the short–distance range corresponding to extensive particles interpenetration. However, only pairs of ellipsoids with large m populate the bins of $g(r)$ with $r \ll \sigma_0$ (i.e., only the softest particles may have significant overlap). The two insets in Figure 4 show that particle softness does not determine significant changes, with respect to the standard model, in the radial distribution functions parallel to the director $g(r_\parallel)$. This is also the case for the perpendicular ones $g(r_\perp)$ apart for a modest population increase in the $r \ll \sigma_0$ bins.

In summary, these MD simulation results suggest that there are two competing effects with opposite influence on the mesogenic properties of elongated GBSC ellipsoids: (a) the softness allows an easier (lower energy) anisotropic close packing into mesogenic structures; and (b) the softness also mellows the effective anisotropy of the GBSC potential by widening the potential energy surface accessible at any given $k_B T$. These features affect the phase diagrams for all SC parametrisations studied in this work (see Figure 5), like the N sample of Figure 6, with $\langle R_{0,0}^2 \rangle = 0.871 \pm 0.001$, formed by uniaxial GBSC ellipsoids of softness $m = -30\,\epsilon_0\,\sigma_0^{-1}$ at a dimensionless temperature $T/(k_B^{-1}\epsilon_0) = 2.2$ (the corresponding standard uniaxial GB system[34] is smectic). We therefore conclude that the softness of the potential can be effectively

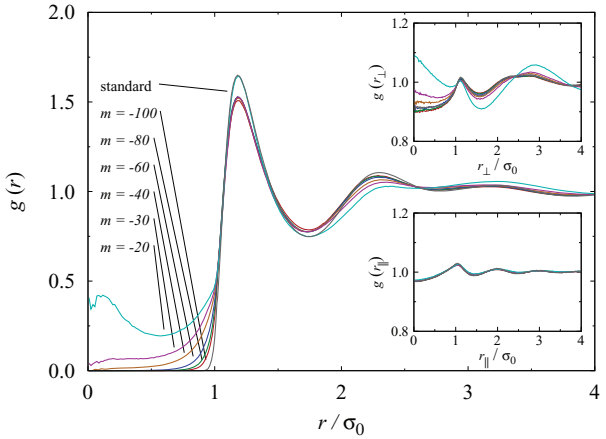

FIG. 4. The radial correlation function $g(r)$ for nematic phases with similar orientational order parameter $\langle R^2_{00}\rangle \approx 0.8$ formed by standard and GBSC uniaxial ellipsoids of various softness $m/(\epsilon_0\,\sigma_0^{-1}) = -100$, -80, -60, -40, -30, and -20 at dimensionless temperatures $T/(k_B^{-1}\epsilon_0) = 2.8$, 3.5, 3.3, 3.1, 2.8, 2.6, and 2.3 as described in the text. The radial distribution functions parallel ($g(r_\parallel)$), and perpendicular ($g(r_\perp)$) to the director are shown in the insets. (See the legend of Figure 2 for additional details.)

tuned to either widen or narrow the nematic temperature range by means of producing both kind of order enhancing or order depressing effects, or even to closely match the mesogenic properties of the standard core GB model. We therefore predict that for surface–stabilised colloidal particles, with solvent responsive surface treatments (such as polymer brushes), it should be possible to both stabilise or destabilise nematic phase formation, simply by choice of appropriate solvent conditions.

B. Biaxial particles

Biaxial GB ellipsoids allow for the tendency of molecules to align along two mutually perpendicular axes, one of which

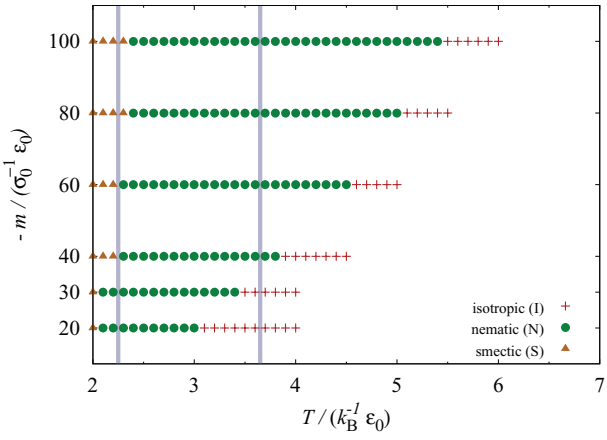

FIG. 5. The phase diagrams plotted against dimensionless temperature $T/(k_B^{-1}\epsilon_0)$ for the uniaxial GBSC ellipsoids of various softness $m/(\epsilon_0\,\sigma_0^{-1}) = -100$, -80, -60, -40, -30, and -20 as described in the text. Samples in the isotropic (I), nematic (N), and smectic (S_m) phases are represented as crosses, circles, and triangles. The I–N and N–S_m transition temperatures for the standard uniaxial GB model (see Ref. 34) are plotted as vertical grey bars. (See the legend of Figure 2 for additional details.)

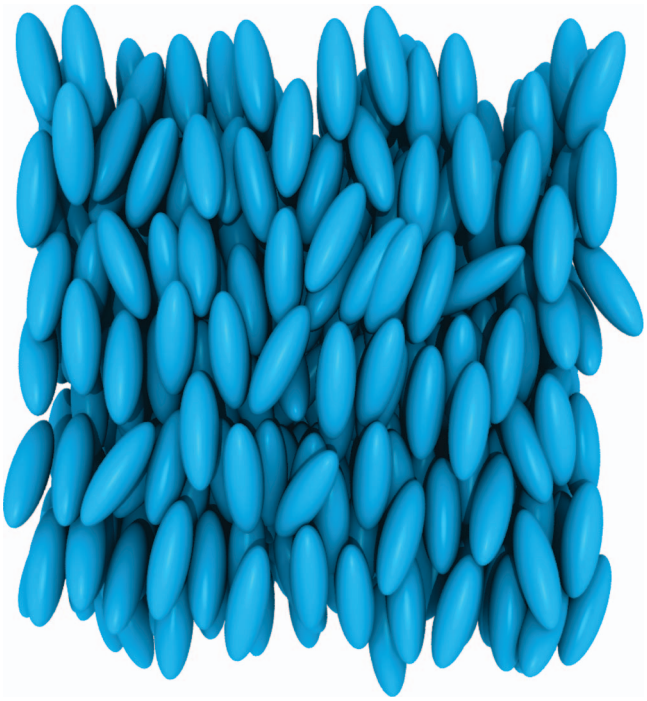

FIG. 6. Snapshot of an N sample for the uniaxial GBSC ellipsoids of softness $m = -30\,\epsilon_0\,\sigma_0^{-1}$ at $T/(k_B^{-1}\epsilon_0) = 2.2$, and $\langle R^2_{0,0}\rangle = 0.871 \pm 0.001$.

may become a macroscopic secondary director for a nematic or smectic phase. (Although biaxial is the normal term employed in soft matter physics, accordingly to the standard crystallographic terminology, such a macroscopically biaxial phase would actually be called triaxial.) To this purpose, we have simulated a second family of GBSC particles based on standard biaxial GB ellipsoids showing isotropic, nematic, biaxial nematic, and biaxial smectic phases (described in Ref. 35).

The general thermodynamic behaviour of these systems of biaxial GBSC ellipsoids resembles that of the uniaxial ones discussed previously. As seen with uniaxial molecules, a small softening of the potential shifts the I–N equilibrium to higher temperatures (29% and 11% for $m = -100\,\epsilon_0\,\sigma_0^{-1}$, and $m = -80\,\epsilon_0\,\sigma_0^{-1}$), an intermediate value gives a T_{IN} matching the standard core model (-6% for $m = -60\,\epsilon_0\,\sigma_0^{-1}$), and a large softness shifts the I–N transition to lower temperatures (-23% and -34% for $m = -40\,\epsilon_0\,\sigma_0^{-1}$, and $m = -30\,\epsilon_0\,\sigma_0^{-1}$). All spontaneous ordering transitions appear to be of very weak first order (or second order nature) since there are no significant discontinuities in the energy or order parameters with temperature. (We note that the biaxial GBSC system with $m = -20\,\epsilon_0\,\sigma_0^{-1}$ does not form a nematic phase upon cooling, so these results have not been included here.) As a general trend we see that the specific behaviour of these model biaxial mesogens changes with softness and is subtly different from what observed in the uniaxial case (see supplementary material[46]). All average dimensionless energies $\langle U\rangle/\epsilon_0$ in the isotropic and nematic phases are higher than those for the standard GB model, and they are not overlapped (see Figure 7(a)). As before, a small degree of softness ($m = -100\,\epsilon_0\,\sigma_0^{-1}$, and $m = -80\,\epsilon_0\,\sigma_0^{-1}$) stabilises the ordered phases, and the I–N transition for these

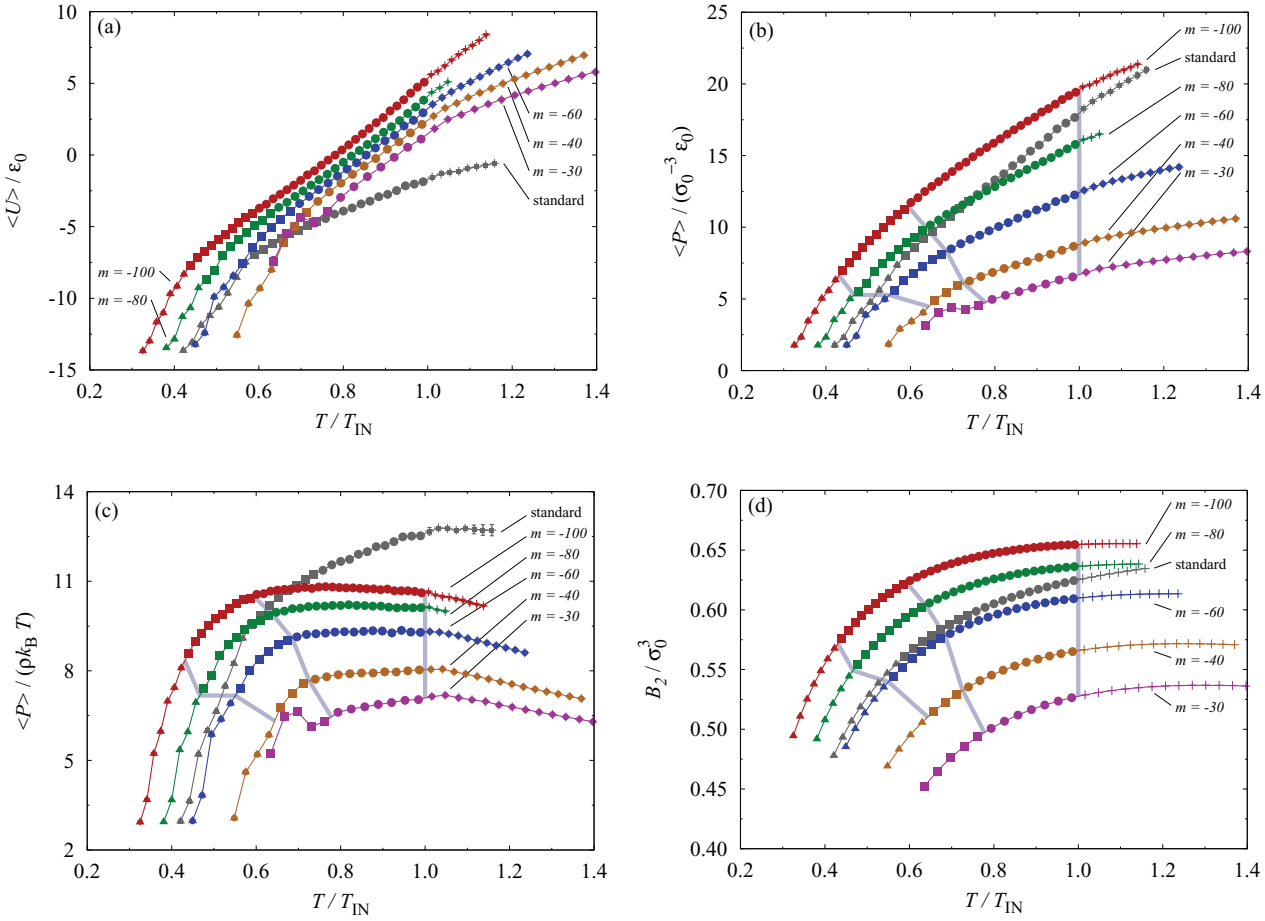

FIG. 7. The average dimensionless potential energy $\langle U \rangle / \epsilon_0$ (plate A), pressure $\langle P \rangle / (\sigma_0^{-3} \epsilon_0)$ (plate B), compressibility factor $\langle P \rangle / (\rho k_B T)$ (plate C), and second virial coefficient B_2 (plate D) plotted as a functions of reduced temperature T / T_{IN} for biaxial ellipsoids modelled either with the standard GB potential (see Ref. 35) or the GBSC parametrisation described in the text. The soft–core energy slopes were $m/(\epsilon_0 \sigma_0^{-1}) = -100$, -80, -60, -40, and -30, while the logistic function steepness was $k = -70 \sigma_0^{-1}$. The biaxial system with $m = -20 \epsilon_0 \sigma_0^{-1}$ does not form a nematic phase upon cooling. The points from the NVT MD simulation of the standard biaxial GB model (see Ref. 35) are also plotted. The rms errors computed, as described in the text, from a block average analysis of the simulation results (see supplementary material of Ref. 46) are also plotted as error bars, however their size smaller than that of the symbols makes them hardly visible. For every SC parametrisation studied T_{IN} is the specific nematic–isotropic transition temperature, respectively $T_{IN}/(k_B^{-1} \epsilon_0) = 6.15$, 5.25, 4.45, 3.65, and 3.15. The thick grey lines join the I–N, N–N_b, and N_b–S_b transition temperatures for the GBSC models. The standard biaxial GB model has instead $T_{IN}/(k_B^{-1} \epsilon_0) = 4.75$. The state points have been computed from MD simulations in the NVT ensemble for $N = 1024$ particles samples at dimensionless number density $(N/V) \sigma_0^3 = 0.3$.

models is shifted to higher temperatures (see Figure 8(a)). The intermediate $m = -60 \epsilon_0 \sigma_0^{-1}$ closely matches the standard GB model, while the softer $m = -40 \epsilon_0 \sigma_0^{-1}$, and $m = -30 \epsilon_0 \sigma_0^{-1}$ occur at lower temperatures. The average pressure has a behaviour similar to that observed for the uniaxial model. In particular, $\langle P \rangle / (\sigma_0^{-3} \epsilon_0)$ is higher than the standard model only for $m = -100 \epsilon_0 \sigma_0^{-1}$ (and at low temperature also for $m = -80 \epsilon_0 \sigma_0^{-1}$), while all other parametrisations provide systems with a systematically lower pressure (see Figure 7(b)) than the parent GB. The compressibility factors for the biaxial SC models in the uniaxial nematic region have a very small temperature dependence and are almost constant (see Figure 7(c)), while the $\langle P \rangle / (\rho k_B T)$ ratio for the standard system varies strictly monotonically with T / T_{IN}.

The second virial coefficients, B_2 (in Figure 7(d)), provides additional insights. The $m = -100 \epsilon_0 \sigma_0^{-1}$, and $m = -80 \epsilon_0 \sigma_0^{-1}$ values produce B_2 values larger than those seen in the parent GB system, promoting mesogenic ordering at high temperatures. The $m = -60 \epsilon_0 \sigma_0^{-1}$ system is very close to the standard system and, as expected, the softer potentials consistently show smaller values of B_2. For all SC biaxial parametrisations we see that the plateau in B_2 is essentially reached before T_{IN}.

The effect of softness on the temperature dependence of the order parameters is particularly interesting. We see that for a given T / T_{IN} the values of $\langle R^2_{0,0} \rangle$ have trends similar to those observed for the uniaxial models both with respect to dimensionless (see Figure 8(a)) and reduced (see Figure 8(b)) temperature. In the latter plot we see that the order parameter profiles for the various m are not superimposable within statistical uncertainty of the average values.

The plot of the biaxial order parameter[35] $\langle R^2_{2,2} \rangle = \langle [(\mathbf{x}_i \cdot \mathbf{l})^2 - (\mathbf{x}_i \cdot \mathbf{m})^2 - (\mathbf{y}_i \cdot \mathbf{l})^2 + (\mathbf{y}_i \cdot \mathbf{m})^2]/4 \rangle$, where $\mathbf{m}$, and $\mathbf{l}$ are the secondary directors, and $\mathbf{x}_i$, $\mathbf{y}_i$ are the transverse molecular axes, shows (see Figure 8(c)) that a moderate softness ($m = -100 \epsilon_0 \sigma_0^{-1}$) slightly stabilises the biaxial nematic phase and shifts the N–N_b transition to a higher dimensionless temperature compared to the standard model (≈3%),

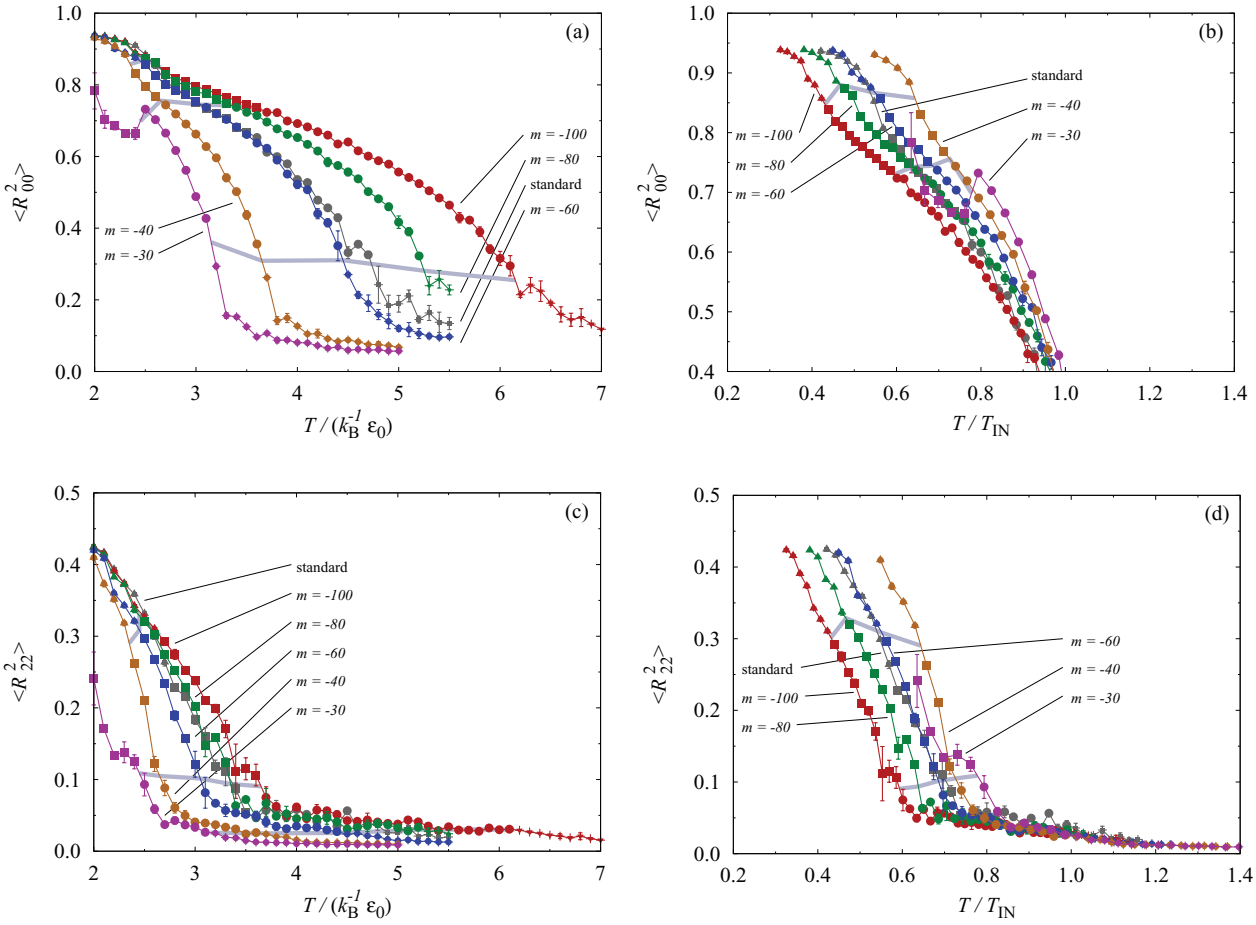

FIG. 8. The orientational order parameters $\langle R^2_{00} \rangle$ and $\langle R^2_{22} \rangle$ plotted against dimensionless temperature $T/(k_B^{-1}\epsilon_0)$ (plate A, uniaxial; plate C, biaxial), and reduced temperature T/T_{IN} (plate B, uniaxial; plate D, biaxial), for the biaxial GBSC ellipsoids of various softness $m/(\epsilon_0\,\sigma_0^{-1}) = -100$, -80, -60, -40, and -30 as described in the text. (See the legend of Figure 7 for additional details.)

while for the $m/(\epsilon_0\,\sigma_0^{-1}) = -80$, -60, -40, and -30 models this transition shifts to lower temperatures (respectively, $\approx -6\%$, $\approx -14\%$, $\approx -25\%$, and $\approx -31\%$). The variation of $\langle R^2_{2,2} \rangle$ with T/T_{IN} (see Figure 8(d)) reveals again that also the biaxial GBSC parametrisations are not corresponding to the same general model, and that different m values provide both higher and lower $\langle R^2_{2,2} \rangle$ at the same reduced temperature compared to the standard biaxial model. We notice that the low–temperature trend of $\langle R^2_{2,2} \rangle$ for $m = -30\,\epsilon_0\,\sigma_0^{-1}$ shows a drop in biaxiality which hints to possible equilibration problems for these samples. For this slope m we have not found layered smectic organisations within the range of explored temperatures.

A summary of the properties of these biaxial GBSC systems can be extracted from the phase diagrams of Figure 9. We find that particle softness provides a high degree of tuning for a thermotropic biaxial nematic phase: taking the parent GB model as reference, the particle softness can extend the stability of the N_b phase to lower temperatures, widen or narrow the biaxial nematic range (Figure 9), or even provide larger values of the $\langle R^2_{2,2} \rangle$ order parameter. An example of this is given by the snapshot of Figure 10 showing a N_b sample, with $\langle R^2_{0,0} \rangle = 0.831 \pm 0.001$, and $\langle R^2_{2,2} \rangle = 0.262 \pm 0.004$, formed by GBSC ellipsoids of softness $m = -40\,\epsilon_0\,\sigma_0^{-1}$ at a dimensionless temperature $T/(k_B^{-1}\epsilon_0) = 2.4$ (the corresponding standard biaxial GB system[35] is well within the S_b phase).

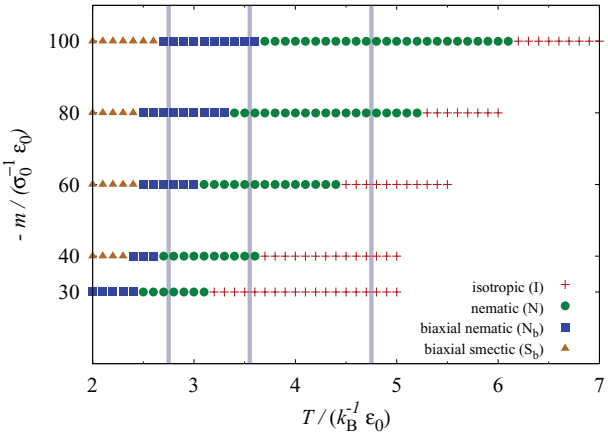

FIG. 9. The phase diagrams plotted against dimensionless temperature $T/(k_B^{-1}\epsilon_0)$ for the biaxial GBSC ellipsoids of various softness $m/(\epsilon_0\,\sigma_0^{-1}) = -100$, -80, -60, -40, and -30 as described in the text, and in the legend of Figure 7. Samples in the isotropic (I), nematic (N), biaxial nematic (N_b), and biaxial smectic (S_b) phases are represented as crosses, circles, squares, and triangles. The I–N, N–N_b, and N_b–S_b transition temperatures for the standard biaxial GB model (see Ref. 35) are plotted as vertical grey bars.

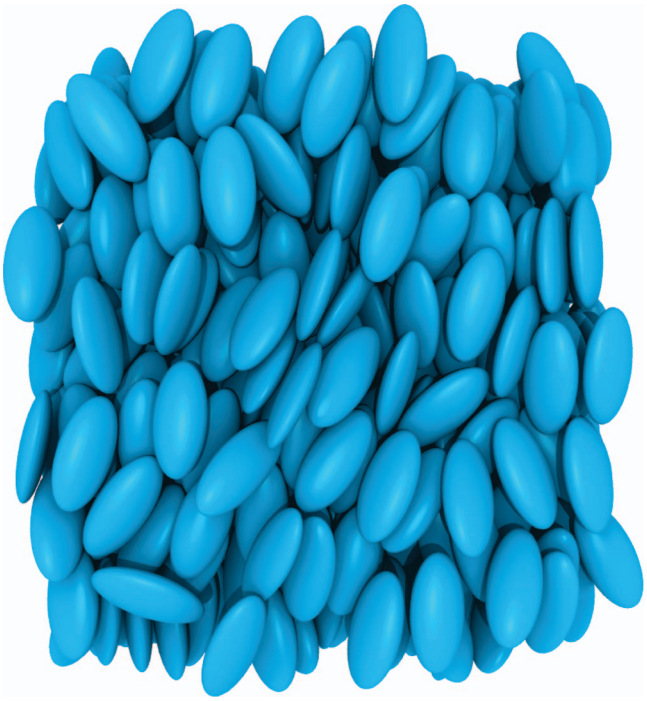

FIG. 10. Snapshot of a N_b sample for the biaxial GBSC ellipsoids of softness $m = -40\,\epsilon_0\,\sigma_0^{-1}$ at $T/(k_B^{-1}\epsilon_0) = 2.4$, $\langle R^2_{0,0}\rangle = 0.831 \pm 0.001$, and $\langle R^2_{2,2}\rangle = 0.262 \pm 0.004$.

It is interesting to note that until quite recent studies[1] it has proved extremely difficult to obtain low molecular weight thermotropic mesogens which exhibit biaxial phases,[49] while such phases have been observed for some time in lyotropic systems.[50] It seems possible that the softness of the typical pair potential seen for the latter, and the subsequent extension of the range of biaxial stability (as seen in this work) is a contributing factor to this. We therefore suggest that the introduction of softness, in the form of conformational flexibility, may be a way to promote biaxiality in low molecular weight thermotropic systems.

IV. CONCLUSIONS

We have determined by MD computer simulations the phase diagrams of two families of uniaxial and biaxial soft–core ellipsoids interacting with a modified anisotropic GB pair potential. These potentials can be considered as appropriate coarse–grained models for a number of systems: very flexible mesogens such as multipodes[1] or dendrimers (where conformational flexibility allows for significant interpenetration of the "*molecular envelopes*"); or soft colloidal mesogenic particles or star polymers.

The MD simulation results show how particle softness affects the mesogenic behaviour by stabilising (moderate degree of softness) or destabilising (large degree of softness) the mesogenic properties, and also by shifting the temperature of the ordering transitions. This effect is particularly pronounced for biaxial particles, and as an important new result we have found that a moderate particle softness actually strongly stabilises low–temperature biaxial nematic organisation against the formation of smectic or crystal phases. Such an effect has been seen in experimental reports of the formation of a low temperature biaxial nematic in a class of flexible siloxane tetrapodes.[1] For systems of colloidal particles stabilised by surface treatment, particle softness can often be made to be highly sensitive to the quality of the solvent. Such systems would provide an interesting experimental test of the predictions made here, and may well lead to solvent tunable biaxial phases. For thermotropics, this work points to the possibility of using semi–flexible (possibly deformable) mesogens, which can form soft particles with a biaxial shape. Such systems, may prove to be another possible architecture for designing room temperature thermotropic biaxial nematics.

Finally, we note that anisotropic soft–core potentials, such as the ones studied in this work, are likely to have a wide range of future potential applications in soft matter physics. In systems as diverse as colloids, star polymers, soft deformable nanoparticles, liquid crystals and microgels, particle softness can play a key role in determining self–assembling and physical properties.

ACKNOWLEDGMENTS

R.B. and C.Z. thank the EU–STREP project "Biaxial Nematic Devices" (BIND) FP7–216025 for financial support, and the CINECA computing centre for computer time. M.R.W. wishes to thank the CINECA computing centre and the HPC Europa2 initiative for financial support for a visit helping to make this work possible.

[1] K. Merkel, A. Kocot, J. K. Vij, R. Korlacki, G. H. Mehl, and T. Meyer, Phys. Rev. Lett. **93**, 237801 (2004).
[2] J. L. Figueirinhas, C. Cruz, D. Filip, G. Feio, A. C. Ribeiro, Y. Frère, T. Meyer, and G. H. Mehl, Phys. Rev. Lett. **94**, 107802 (2005).
[3] C. N. Likos, H. Löwen, M. Watzlawek, B. Abbas, O. Jucknischke, J. Allgaier, and D. Richter, Phys. Rev. Lett. **80**, 4450 (1998).
[4] S. Nayak and L. A. Lyon, Angew. Chem., Int. Ed. **44**, 7686 (2005).
[5] A. S. J. Iyer and L. A. Lyon, Angew. Chem., Int. Ed. **48**, 4562 (2009).
[6] J. Mattsson, H. M. Wyss, A. Fernandez-Nieves, K. Miyazaki, Z. Hu, D. R. Reichman, and D. A. Weitz, Nature (London) **462**, 83 (2009).
[7] M. Ballauff and C. N. Likos, Angew. Chem., Int. Ed. **43**, 2998 (2004).
[8] A. Stradner, H. Sedgwick, F. Cardinaux, W. C. K. Poon, S. U. Egelhaaf, and P. Schurtenberger, Nature (London) **432**, 492 (2004).
[9] Z. Yang, W. T. S. Huck, S. M. Clarke, A. R. Tajbakhsh, and E. M. Terentjev, Nature Mater. **4**, 486 (2005).
[10] K. R. Purdy, S. Varga, A. Galindo, G. Jackson, and S. Fraden, Phys. Rev. Lett. **94**, 057801 (2005).
[11] C. M. Care and D. J. Cleaver, Rep. Prog. Phys. **68**, 2665 (2005).
[12] D. J. Earl, J. Ilnytskyi, and M. R. Wilson, Mol. Phys. **99**, 1719 (2001).
[13] J. S. Lintuvuori and M. R. Wilson, J. Chem. Phys. **128**, 044906 (2008).
[14] Z. E. Hughes, L. M. Stimson, H. Slim, J. S. Lintuvuori, J. M. Ilnytskyi, and M. R. Wilson, Comput. Phys. Commun. **178**, 724 (2008).
[15] J. M. Ilnytskyi, J. S. Lintuvuori, and M. R. Wilson, Condens. Matter Phys. **13**, 33001 (2010).
[16] S. Sarman, J. Chem. Phys. **107**, 3144 (1997).
[17] S. Sarman and A. Laaksonen, Phys. Chem. Chem. Phys. **13**, 5915 (2011).
[18] D. Andrienko, G. Germano, and M. P. Allen, Phys. Rev. E **63**, 041701 (2001).
[19] N. Akino, F. Schmid, and M. P. Allen, Phys. Rev. E **63**, 041706 (2001).
[20] S. Prestipino, F. Saija, and P. V. Giaquinta, Phys. Rev. E **71**, 050102 (2005).
[21] S. Prestipino and F. Saija, J. Chem. Phys. **126**, 194902 (2007).
[22] A. Nikoubashman and C. N. Likos, J. Phys. Condens. Matter **22**, 104107 (2010).
[23] J. G. Gay and B. J. Berne, J. Chem. Phys. **74**, 3316 (1981).
[24] R. Berardi, C. Fava, and C. Zannoni, Chem. Phys. Lett. **236**, 462 (1995).
[25] R. Berardi, C. Fava, and C. Zannoni, Chem. Phys. Lett. **297**, 8 (1998).

[26]M. R. Wilson, Int. Rev. Phys. Chem. **24**, 421 (2005).
[27]M. R. Wilson, Chem. Soc. Rev. **36**, 1881 (2007).
[28]R. Berardi, L. Muccioli, S. Orlandi, M. Ricci, and C. Zannoni, J. Phys.: Condens. Matter **20**, 463101 (2008).
[29]R. Berardi, C. Zannoni, J. S. Lintuvuori, and M. R. Wilson, J. Chem. Phys. **131**, 174107 (2009).
[30]G. Skačej and C. Zannoni, "Main-chain swollen liquid crystal elastomers: a molecular simulation study," Soft Matter (in press).
[31]A. George and W. W. Wilson, Acta Crystallogr., Sect. D: Biol. Crystallogr. **50**, 361 (1994).
[32]G. A. Vliegenthart and H. N. W. Lekkerkerker, J. Chem. Phys. **112**, 5364 (2000).
[33]N. M. Dixit and C. F. Zukoski, J. Colloid Interface Sci. **228**, 359 (2000).
[34]R. Berardi, A. P. J. Emerson, and C. Zannoni, J. Chem. Soc., Faraday Trans. **89**, 4069 (1993).
[35]R. Berardi and C. Zannoni, J. Chem. Phys. **113**, 5971 (2000).
[36]M. P. Allen and G. Germano, Mol. Phys. **104**, 3225 (2006).
[37]R. Berardi, L. Muccioli, and C. Zannoni, J. Chem. Phys. **128**, 024905 (2008).
[38]P. D. Duncan, A. J. Masters, and M. R. Wilson, Phys. Rev. E **84**, 011702 (2011).
[39]F. J. Martínez–Veracoechea and F. A. Escobedo, J. Chem. Phys. **125**, 104907 (2006).
[40]M. Marechal, A. Cuetos, B. Martínez–Haya, and M. Dijkstra, J. Chem. Phys. **134**, 094501 (2011).
[41]D. Frenkel and B. Smit, *Understanding Molecular Simulations: From Algorithms to Applications*, 2nd ed. (Academic, San Diego, 2001).
[42]N. Matubayasi and M. Nakahara, J. Chem. Phys. **110**, 3291 (1999).
[43]H. Kamberaj, R. J. Low, and M. P. Neal, J. Chem. Phys. **122**, 224114 (2005).
[44]H. J. C. Berendsen, J. P.M. Postma, W. F. van Gunsteren, A. DiNola, and J. R. Haak, J. Chem. Phys. **81**, 3684 (1984).
[45]E. Paci and M. Marchi, J. Phys. Chem. **100**, 4314 (1996).
[46]See supplementary material at http://dx.doi.org/10.1063/1.3646310 for the tables of the average orientational order parameters $\langle R^2_{00}\rangle$, and $\langle R^2_{22}\rangle$, dimensionless potential energy per particle $\langle U\rangle/\epsilon_0$, and dimensionless pressure $\langle P\rangle/(\sigma_0^{-3}\epsilon_0)$ for the various GBSC model potentials.
[47]S. Yadav, T. M. Scherer, S. J. Shire, and D. S. Kalonia, Anal. Biochem. **411**, 292 (2011).
[48]J. M. Mollerup and M. P. Breil, Fluid Phase Equilib. **286**, 88 (2009).
[49]C. Tschierske and D. J. Photinos, J. Mater. Chem. **20**, 4263 (2010).
[50]L. J. Yu and A. Saupe, Phys. Rev. Lett. **45**, 1000 (1980).